Int. J. Therm. Sci. (2000) 39, 949–960

S1290-0729(00)01176-5/FLA

Thermodynamic optimization of geometry: T- and Y-shaped constructs of fluid streams

A. Bejan [a]*, L.A.O. Rocha [a], S. Lorente [b]

[a] *Duke University, Department of Mechanical Engineering and Materials Science, Durham, NC 27708-0300, USA*

[b] *INSA Toulouse, Department of Civil Engineering, Scientific Complex of Rangueil, 135 Av. Rangueil, 31077 Toulouse, France*

(Received 19 May 2000, accepted 10 July 2000)

Abstract — This paper presents a series of examples in which the global performance of flow systems is optimized subject to global constraints. The flow systems are assemblies of ducts, channels and streams shaped as Ts, Ys and crosses. In pure fluid flow, thermodynamic performance maximization is achieved by minimizing the overall flow resistance encountered over a finite-size territory. In the case of more complex objectives such as the distribution of a stream of hot water over a territory, performance maximization requires the minimization of flow resistance and the leakage of heat from the entire network. Taken together, these examples show that the geometric structure of the flow system springs out of the principle of global performance maximization subject to global constraints. Every geometric detail of the optimized flow structure is deduced from principle. The optimized structure (design, architecture) is robust with respect to changes in some of the parameters of the system. The paper shows how the geometric optimization method can be extended to other fields, e.g., urban hydraulics and, in the future, exergy analysis and thermoeconomics.

thermodynamic optimization / topology optimization / structure / tree networks / constructal

Nomenclature

a, b	variables	
A	area	m^2
A_c	cross-sectional area	m^2
$c_{1,2}$	constants	
c_p	specific heat at constant pressure	$J \cdot kg^{-1} \cdot K^{-1}$
d	depth	m
D	diameter, channel width	m
f	friction factor	
F	geometric group	
h	heat transfer coefficient	$W \cdot m^{-2} \cdot K^{-1}$
k	thermal conductivity	$W \cdot m^{-1} \cdot K^{-1}$
L	length	m
$\dot{m}$	mass flow rate	$kg \cdot s^{-1}$
p	perimeter	m
q'	heat transfer rate per unit length	$W \cdot m^{-1}$
r, R	geometric groups	
$r_{i,o}$	inner and outer radii of insulation	m
t_w	wall thickness	m
T	temperature	K
T_0	inlet temperature	K
T_∞	ambient temperature	K
U	mean velocity	$m \cdot s^{-1}$
V	volume	m^3
x, y	variables	
x, y	Cartesian coordinates	m
z	elevation	m

Greek symbols

α, β	angles	rad
ΔP	pressure drop	Pa
ν	kinematic viscosity	$m^2 \cdot s^{-1}$
ρ	density	$kg \cdot m^{-3}$

Subscripts

j	junction
min	minimum
opt	optimum
out	outlet
$\sim$	dimensionless variables, equations (42)

* Correspondence and reprints.
abejan@duke.edu

1. THERMODYNAMIC OPTIMIZATION OF GEOMETRY

Among the more recent methods that have become established in thermal engineering, thermodynamic optimization has the objective of improving the global performance of the system subject to specified global constraints. Improvement means the decrease in the irreversibility (or entropy generation, exergy destruction) that characterizes all the components and processes of the system. Thermodynamic optimization is useful as a first step, for orientation in the search of tradeoffs that govern the geometric configuration of the system. This knowledge is useful later, as guidelines in the development of more complex and realistic models, and in the final design optimization that is based on cost minimization [1].

An engineering flow system owes its irreversibility to several mechanisms, most notably the flow of heat, fluid and electric current against finite resistances. The entropy generated by each current is proportional to the product of the current times the driving potential (e.g., pressure difference) [1, 2], i.e. proportional to the resistance overcome by the current. In simple terms, the entire effort to optimize thermodynamically the greater system rests on the ability to minimize all the internal flow resistances, together. Resistances cannot be minimized individually and indiscriminately, because of constraints: space is limited, streams must connect components, and components must "fit" inside the greater system. Because of constraints, the resistances compete against each other.

The route to improvements in global performance is by *balancing* the reductions in the competing resistances. Thermodynamically, this amounts to spreading the entropy generation rate through the system in an optimal way, so that the total irreversibility is reduced. Optimal spreading is achieved by properly sizing, shaping and positioning the components. Optimal spreading means geometry. In the end, the geometric structure of the system — its architecture — emerges as a result of global thermodynamic optimization.

The generation of system structure by global optimization is, of course, complicated and opaque to the observer's eye when the systems and its functions are complex. It is simpler and easier to see when the system houses only a few streams, as in the fluid-flow examples treated in the present paper. These examples belong to the wide class of engineering and natural flows that connect an infinity of points (volume, area) to one or more discrete points (sources, sinks). All the volume-point flows are shaped as trees. Natural examples are the river basins and deltas, lungs, vascularized tissues, botanical trees, and leaves. Manmade flows shaped as trees are found in the cooling systems of electronics packages and windings of electric machines, regenerative heat exchangers, street and traffic patterns, and networks for distributing city water and for collecting rainwater and sewage.

Tree-shaped flows have been studied extensively in physiology, geophysics and engineering. To review this large body of work is not the purpose of this article; book-size reviews can be found in [3–6]. The work described in this paper was stimulated by a series of recent articles that showed that tree networks and other geometric forms of flow systems can be derived from the optimization of global performance subject to global constraints [7–10].

The form-generating principle was encountered first in heat transfer, in the problem of minimizing the global thermal resistance between a heat-generating volume and a point-size heat sink [7]. This fundamental problem was stimulated by electronics cooling applications at progressively smaller dimensions, where geometric optimization plays an increasingly important role. In the volume-to-point flow problem heat was generated uniformly throughout the volume. A small amount of high-conductivity material was used in the form of thin inserts, to collect the generated heat, and to channel it with minimum resistance to the heat sink.

The geometric optimization consisted of choosing the best thicknesses, shapes and positions for the high-conductivity inserts. This work was done at several volume scales, starting with the smallest and proceeding toward larger scales (assemblies, constructs). During this optimization and construction procedure the inserts formed a tree network in which every single geometric feature was a result of the invoked design principle. The method was named "constructal" because of the construction based on optimized building blocks, or the sequence from small to large with optimization at every step.

The method was also applied to systems with fluid flow [8], convection [9], and urban traffic [10]. The engineering contribution of the method is to show that it is possible to arrive at the main features of the optimized architecture in a few steps of geometric optimization. Refinements of the optimized architecture can be pursued subsequently, for example, via numerical simulations of the flow in many configurations that differ only slightly from each other.

In this paper we propose a simpler way of approaching the geometric optimization of tree-shaped paths for fluid flow. Instead of focusing on the volume-point flow and arriving at the tree structure, we consider the much simpler building block consisting of a few streams that

serve as tributaries or branches in a constrained space. For example, a larger stream with two branches (or two tributaries) forms a construct shaped as a T or Y. We show how all the geometric features of the construct can be derived from the global minimization of resistance to flow. We also show that by putting together the optimized constructs it is possible to reconstruct features of the much more complicated tree structures optimized in the past.

2. LAMINAR FLOW IN A T-SHAPED ASSEMBLY OF TUBES

Consider first the case of incompressible flow through the T-shaped structure formed by a tube of length L_1 and diameter D_1, which is continued by two tubes of length L_2 and diameter D_2. The stream $\dot{m}$ may flow in the direction shown in *figure 1*, or it may flow in the opposite direction. The flow through each tube is laminar and fully developed (Hagen–Poiseuille). The total volume occupied by the tubes is fixed,

$$\frac{\pi}{4}\left(D_1^2 L_1 + 2D_2^2 L_2\right) = \text{const} \tag{1}$$

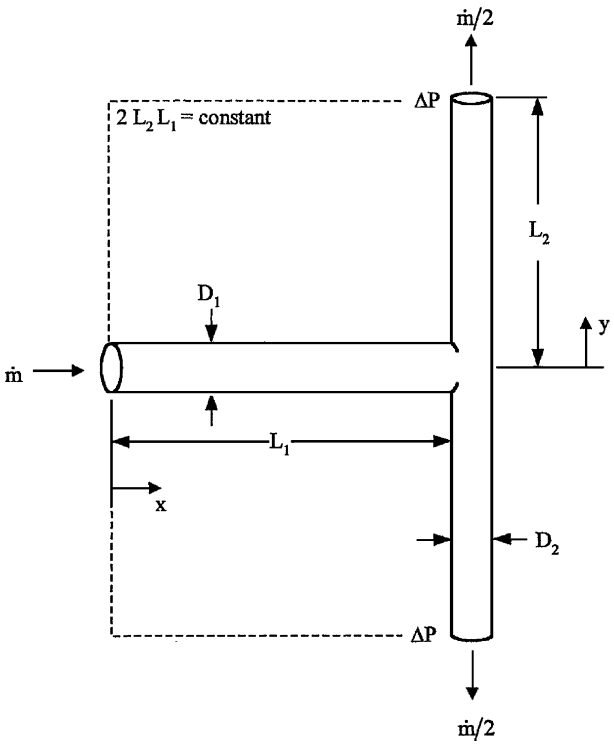

Figure 1. T-shaped assembly of round tubes.

Fixed is also the total space occupied by the planar structure,

$$2L_2 L_1 = A = \text{const} \tag{2}$$

The objective is to minimize the global flow resistance encountered by the stream $\dot{m}$. This is achieved geometrically, by selecting the proper aspect ratios that define the architecture (D_2/D_1, L_2/L_1).

The relation between mass flow rate $\dot{m}$ and end-to-end pressure drop ΔP in fully developed laminar flow through a tube of inner diameter D and length L is

$$\frac{\Delta P}{\dot{m}} = \frac{128}{\pi}\frac{\nu L}{D^4} \tag{3}$$

The flow resistance $\Delta P/\dot{m}$ is proportional to the geometric ratio L/D^4. For the sake of brevity, in the following analysis we write L/D^4 for flow resistance, instead of the full expression (3).

The stream flows through a resistance $R_1 = L_1/D_1^4$ and continues through (or comes from) two branches of resistance $R_2 = L_2/D_2^4$. The R_2 resistances are in parallel; their overall effect is the resistance R_3 given by

$$\frac{1}{R_3} = \frac{1}{R_2} + \frac{1}{R_2} \tag{4}$$

which yields $R_3 = R_2/2$. The R_1 and R_3 resistances are in series; their total resistance is $R = R_1 + R_3$, or

$$R = \frac{L_1}{D_1^4} + \frac{L_2}{2D_2^4} \tag{5}$$

The internal volume of each tube is proportional to $D^2 L$. For brevity, instead of equation (1) we account for the total tube volume by writing

$$V = L_1 D_1^2 + 2L_2 D_2^2 \tag{6}$$

We seek to minimize the total resistance (5) subject to the volume constraint (6). The geometric optimization proceeds in two stages. In the first we optimize the "internal" aspect ratio D_2/D_1. For this we use the notation

$$x = D_1^2, \qquad y = D_2^2 \tag{7}$$

such that equations (5) and (6) become

$$R = \frac{L_1}{x^2} + \frac{L_2}{2y^2} \tag{8}$$

$$V = L_1 x + 2L_2 y \tag{9}$$

Next, we eliminate y from equation (9), $y = a - bx$, where $a = V/(2L_2)$ and $b = L_1/(2L_2)$, and R becomes

$$R = \frac{L_1}{x^2} + \frac{L_2}{2(a-bx)^2} \tag{10}$$

The R minimum is found by solving $\mathrm{d}R/\mathrm{d}x = 0$, which in combination with $b = L_1/(2L_2)$ yields $(a - bx)/x = 2^{-2/3}$. Substituting this result into the preceding relations we find $y/x = 2^{-2/3}$ and, in order,

$$\frac{D_2}{D_1} = 2^{-1/3} \tag{11}$$

$$R_{\min} = \frac{1}{x^2}\left(L_1 + 2^{1/3}L_2\right) \tag{12}$$

$$V = x\left(L_1 + 2^{1/3}L_2\right) \tag{13}$$

$$R_{\min}V^2 = \left(L_1 + 2^{1/3}L_2\right)^3 \tag{14}$$

The ratio of successive tube diameters (11) is an old result, which in physiology is known as Murray's law [11, 12]. For us it marks the end of the first step of geometric optimization. This result is remarkable for its robustness: the optimal ratio D_2/D_1 is independent of the assumed tube lengths (L_1, L_2). It is also independent of the relative position of the tubes — the layout of the T-shaped structure. It is independent of geometry.

The next step is new: we minimize $R_{\min}$ at constant V by selecting the lengths L_1 and L_2. According to equation (14), it is sufficient to minimize the expression

$$r = L_1 + 2^{1/3}L_2 \tag{15}$$

subject to the area constraint — the territory — allocated to the three tubes, equation (2). The minimization of r subject to constant A yields the tube lengths

$$L_1 = 2^{-1/3}A^{1/2}, \qquad L_2 = 2^{-2/3}A^{1/2} \tag{16}$$

and their ratio

$$\frac{L_2}{L_1} = 2^{-1/3} \tag{17}$$

In conclusion, equations (11) and (17) show that at the junction the tube lengths and diameters change in the same proportion. This also means that each tube is geometrically similar to its tributary or collector, $D_1/L_1 = D_2/L_2$. We return to this observation at the end of the next section.

3. TURBULENT FLOW IN A T-SHAPED ASSEMBLY OF CHANNELS

The purpose of the preceding example was to illustrate the method and its analytical steps. In this section and the remainder of the paper we report the solutions to a class of related problems. For brevity, we omit the analytical details, and highlight only the features that are new relative to the steps undertaken in section 2.

In the T-shaped assembly of *figure 2* we have made three changes:

(i) The flow is in the fully-rough turbulent regime, so that the friction factor may be approximated by a constant for all the channels. Turbulent flows are especially encountered in civil engineering applications such as hydraulics, hot water distribution and heating, and air conditioning.

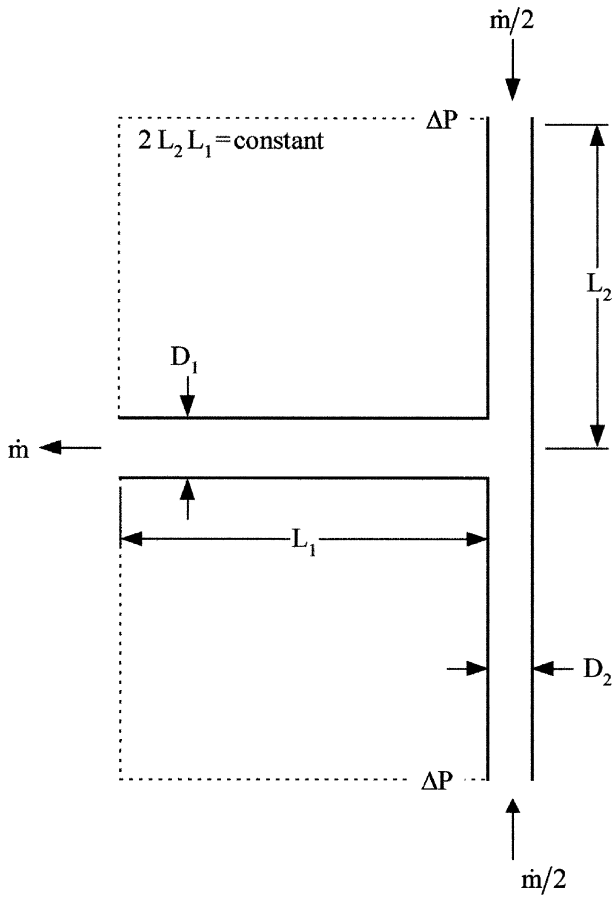

Figure 2. T-shaped assembly of closed or open channels.

(ii) The channel cross-section may have several shapes (round, parabolic, triangular, rectangular), and the stream may even have a free surface (open channel flow).

(iii) The flow may be driven by differences in elevation (i.e. gravity), or by the pressure difference ΔP shown in *figure 2*.

Regarding (iii), there is a useful analogy between gravity- and pressure-driven flows. For example, the flow through each river channel is driven by the slope of the channel, i.e. by the gravitational acceleration component aligned with the channel. In steady flow this body force is balanced by the longitudinal friction force integrated over the wetted surface of the channel. The force balance provides a relation between the channel slope and the flow rate or mean velocity of the stream: this relation will be presented in the next section, where it will be clear that the channel slope plays the same role as the pressure drop ΔP maintained between the ends of a duct with through flow. We develop the solution in terms of ΔP, so that its results can also be applied to completely enclosed streams (ducts) with turbulent flow.

The geometry of the assembly of *figure 2* has three degrees of freedom, which are optimized in this order: the shape of the channel cross-section, the internal aspect ratio D_2/D_1, and the external aspect ratio L_2/L_1. Assume that A_c and p are the area and wetted perimeter of the channel cross-section. The force balance for a channel of length L and mean velocity U yields

$$\Delta P = f\,\frac{pL}{A_c}\left(\frac{1}{2}\,\rho U^2\right) \tag{18}$$

In the fully rough turbulent limit the friction factor f is essentially constant, i.e. independent of Reynolds number or flow rate. The flow rate is $\dot{m} = \rho U A_c$. Let D represent the transversal dimension — the width — of the duct or channel. Accordingly, $p = \pi D$ for the round duct and $p = \pi D/2$ for the open channel with half-disk cross-section.

A rectangular cross-section has two dimensions, the width D and depth d. To minimize the flow resistance of equation (18) by varying the cross-sectional shape means to minimize the wetted perimeter p subject to fixed A_c. If the rectangular flow cross-section does not have a free surface, then $p = 2(D + d)$, and the optimal shape subject to $A_c = dD$, constant, is the square, $d/D = 1$. If the rectangular cross-section houses an open channel flow of depth d, then $p = D + 2d$, and the optimal cross-sectional shape is $d/D = 1/2$. Similarly, we find that the optimal shape of a triangular cross-section with D-wide free surface and maximum depth d is represented by $d/D = 1/2$.

Putting these optimal cross-sectional shapes together, including the round duct and the open channel flow with half-disk cross-section, we conclude that the result of optimizing the stream cross-section is a wetted perimeter p that scales with D, and a cross-sectional area A_c that is of order D^2. This summary means that equation (18) expresses the proportionality

$$\frac{\Delta P}{\dot{m}^2} \sim r \tag{19}$$

where r is a purely geometric group of the duct or channel,

$$r = \frac{L}{D^5} \tag{20}$$

Unlike in laminar flow (section 2), where ΔP is proportional to $\dot{m}$, in the fully-rough and fully-turbulent regime ΔP is proportional to $\dot{m}^2$.

We now turn our attention to the pressure drop ΔP across the entire assembly of channels. Let ΔP_1 be the pressure drop across the single channel ($\dot{m}, L_1, D_1$), and ΔP_2 the pressure drop across the two channels ($\dot{m}/2, L_2, D_2$ each) connected in parallel. Assuming that the pressure drop due to losses right at the T junction is small when compared with ΔP, we recognize that

$$\Delta P = \Delta P_1 + \Delta P_2 \tag{21}$$

and, after using equation (19), we obtain the global relationship between ΔP and $\dot{m}$ for the assembly:

$$\frac{\Delta P}{\dot{m}^2} \sim r_1 + r_2\left(\frac{\dot{m}/2}{\dot{m}}\right)^2 \tag{22}$$

The right side of equation (22) shows that the object of the geometric minimization effort is the expression

$$R = \frac{L_1}{D_1^5} + \frac{L_2}{4D_2^5} \tag{23}$$

Assume that the total volume occupied by the channels is constrained, equation (6). Using the notation (7), and following the steps shown in equations (8)–(14), we obtain the optimal ratio of channel widths

$$\frac{D_2}{D_1} = 2^{-3/7} \tag{24}$$

$$R_{\min} V^{5/2} = 2^{1/2}\left(2^{-1/7} L_1 + L_2\right)^{7/2} \tag{25}$$

The third minimization of the global resistance is achieved by minimizing the geometric group

$(2^{-1/7}L_1 + L_2)$ subject to the fixed two-dimensional territory A, equation (2). The result is

$$\frac{L_2}{L_1} = 2^{-1/7} \tag{26}$$

This ratio is closer to 1 than the corresponding ratio for ducts with laminar flow, equation (17). Unlike in the laminar case (section 2), in which the geometric similarity ratio D/L was preserved in going from each tube to its branch, in turbulent flow the geometric ratio that is preserved is D/L^3: note that equations (24) and (26) yield $D_1/L_1^3 = D_2/L_2^3$.

4. EQUIPARTITION OF PRESSURE DROP AND ELEVATION

In sections 2 and 3 we minimized the resistance of the three-channel assembly, and obtained two optimal geometric ratios, D_2/D_1 and L_2/L_1. An interesting feature of this optimal design is that the overall pressure drop ΔP is divided exactly in half by the junction point. For example, using equations (24) and (26) in the resistance formula (23), we see that

$$\frac{\Delta P_1}{\Delta P_2} = \frac{L_1/D_1^5}{L_2/4D_2^5} = 1 \tag{27}$$

Similarly, by using equations (11) and (17) in equation (5), we conclude that the equipartition of pressure drop characterizes the optimal design not only in turbulent flow but also in laminar flow.

The preceding geometric results are valid for pressure-driven and gravity-driven flows. The analogy between the two is demonstrated as follows. Assume that the open channel flow driven by gravity is straight, and that the height difference between its ends is z, where $z \ll L$. The channel slope is z/L, the gravitational acceleration component that drives the flow is gz/L, and the total body force that pulls the liquid column through the channel is $(\rho A_c L)gz/L$. This force is balanced by the friction force integrated over all the wetted surface, namely, τpL, where τ is the shear stress $\tau = f(\rho U^2/2)$. The force balance

$$\rho A_c L \frac{gz}{L} = f \frac{1}{2} \rho U^2 pL \tag{28}$$

can be rewritten as

$$\rho gz = f \frac{pL}{A_c}\left(\frac{1}{2}\rho U^2\right) \tag{29}$$

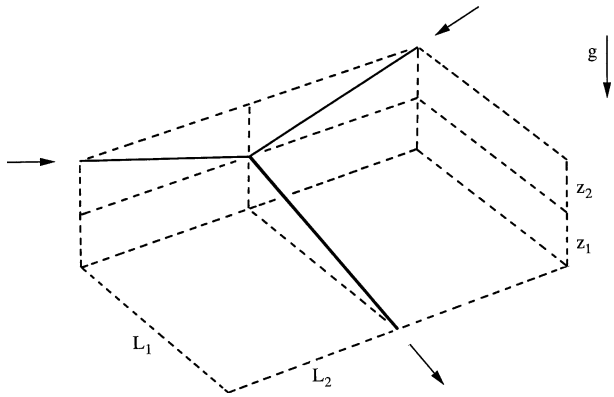

Figure 3. The equipartition of elevation when the T-shaped assemblies of *figures 1* and *2* are optimized geometrically for gravity-driven flow with minimum resistance.

Equations (29) and (18) show that the product ρgz plays the same role as ΔP in duct flow. If z_1 and z_2 are the net drops in elevation along the L_1 and L_2 channels, respectively, then the total drop between the two inlets and the outlet is

$$z = z_1 + z_2 \tag{30}$$

This equation replaces equation (21), and the optimization (18)–(27) applies unchanged. In particular, equation (27) means that the elevation of the junction is exactly half-way between the elevations of the inlet and outlet ports of the assembly. This feature is illustrated in *figure 3*.

5. OPTIMAL ANGLE OF CONFLUENCE IN A Y-SHAPED ASSEMBLY

Further progress on the geometric minimization of flow resistance can be made by relaxing some of the simplifying features used in the T-shaped assemblies. In *figure 4*, for example, we have abandoned the 90° angles between streams. The angle β is variable, and adds itself as a degree of freedom in the optimization of the new Y-shaped assembly.

As in *figure 1*, we assume that the flow is laminar through round tubes, and that the entire construct is housed by a rectangular area A. According to the notation defined on *figure 4*, the area constraint is

$$A = 2L_2 \cos\beta (L_1 + L_2 \sin\beta) \tag{31}$$

The optimized ratio of tube diameters, equation (11), continues to be valid because it is insensitive to changes in the tube lengths. This means that the flow resistance

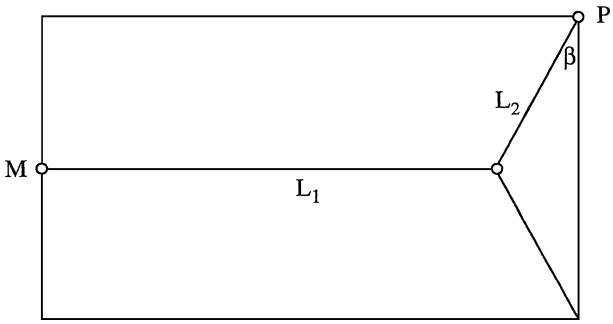

Figure 4. Y-shaped assembly occupying a rectangular area.

to optimize is the expression reported in equation (14), which is minimum for the Y configuration where the group $(L_1 + 2^{1/3}L_2)$ is minimum.

In sum, the optimization of the Y configuration consists of minimizing $(L_1 + 2^{1/3}L_2)$ subject to the area constraint (31), by varying the shape parameters L_1/L_2 and β. First, the optimization with respect to L_1/L_2 yields

$$\frac{L_1}{L_2} = 2^{1/3} - 2\sin\beta \tag{32}$$

relative to which equation (17) is the special case $\beta = 0$, or *figure 1*. Next, by substituting this ratio length in the flow resistance group $(L_1 + 2^{1/3}L_2)$, and using the constraint (31) to eliminate L_1 (or L_2), we obtain

$$L_1 + 2^{1/3}L_2 = \left(2A\,\frac{2^{1/3} - \sin\beta}{\cos\beta}\right)^{1/2} \tag{33}$$

The optimization with respect to β requires the minimization of $(2^{1/3} - \sin\beta)/\cos\beta$, which yields $\sin\beta = 0.794$, or $\beta = 0.917$ rad. The group $L_1 + 2^{1/3}L_2$ decreases monotonically from $\beta = 0$ to 0.917 rad. The angle $\beta = 0.917$ rad does not represent a realistic design, because if we substitute it into equation (32) we obtain a negative L_1. The smallest realistic resistance corresponds to the degenerate Y without a stem ($L_1 = 0$), where the L_2 tubes stretch all the way from the corner P to the root point M (see *figure 4*).

An optimal angle of confluence in a Y-shaped assembly with finite L_1 exists when the shape of the A territory is not free to vary, i.e. when the ratio of tube lengths (L_1/L_2) is disconnected from the aspect ratio of A. As an example, we chose the Y inscribed in a disk-shaped domain. The disk radius r is fixed. The layout of the Y construct is defined by the angles α and β defined in *figure 5*.

Again, the focus of the resistance minimization effort is equation (14), or the group $(L_1 + 2^{1/3}L_2)$. The tube lengths can be expressed in terms of r, α and β:

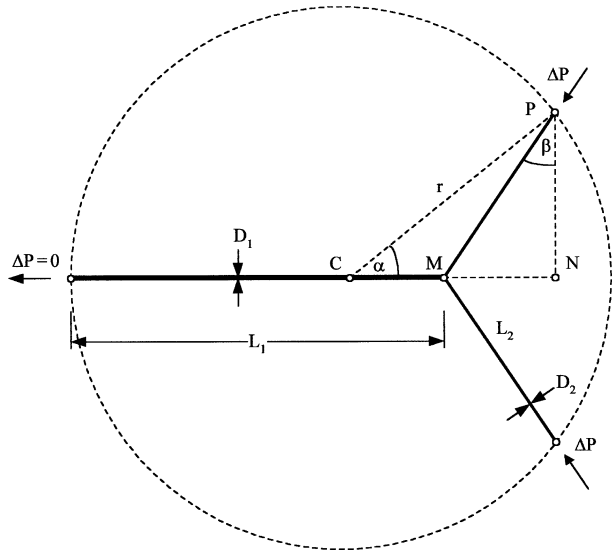

Figure 5. Y-shaped assembly occupying a disk-shaped area.

$$L_2 = r\,\frac{\sin\alpha}{\cos\beta} \tag{34}$$

$$L_1 = r(1 + \cos\alpha - \sin\alpha\tan\beta) \tag{35}$$

Next, we find that the group $(L_1 + 2^{1/3}L_2)$ is proportional to the geometric expression

$$F = 1 + \cos\alpha - \sin\alpha\tan\beta + 2^{1/3}\,\frac{\sin\alpha}{\cos\beta} \tag{36}$$

Solving $\partial F/\partial\alpha = 0$ and $\partial F/\partial\beta = 0$ together, we obtain the optimal angles

$$\alpha = 0.654 \text{ rad}, \qquad \beta = 0.917 \text{ rad} \tag{37}$$

and, consequently, the length ratios:

$$\frac{L_1}{r} = 1, \qquad \frac{L_2}{r} = 1, \qquad \frac{L_2}{L_1} = 1 \tag{38}$$

In this optimal configuration the tubes are connected exactly in the center of the Y-shaped construct. The angle between the two L_2 tubes is very close to 75°. The ratio L_2/L_1 is larger than in the optimized T construct, equation (17).

6. CROSS-SHAPED ASSEMBLY OF TUBES

The same method can be applied to more complicated constructs. More complex than the three-tube assembly of *figure 1* is the four-tube assembly of *figure 6*. As

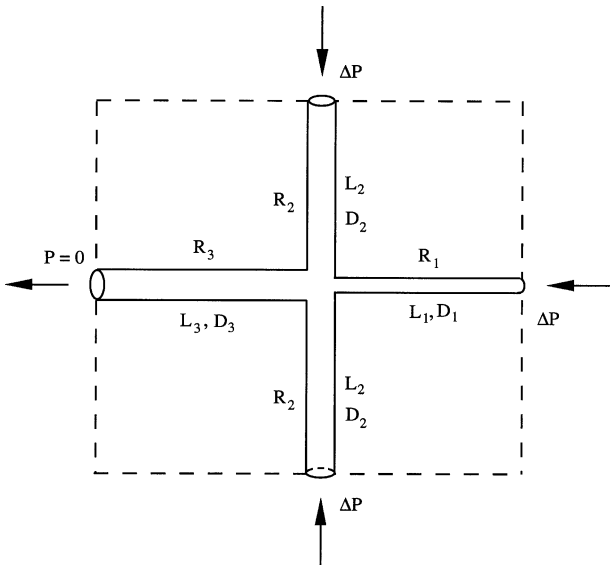

Figure 6. Cross-shaped assembly of round tubes.

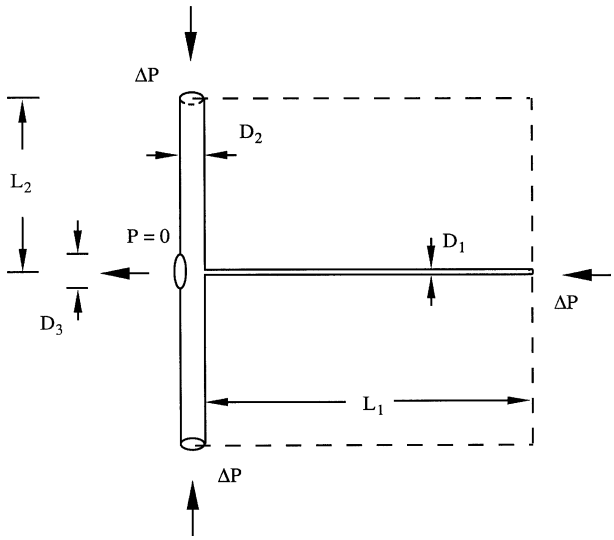

Figure 7. Optimized cross-shaped assembly of tubes when the center of the cross is free to move.

in section 2, the flow is assumed laminar and fully developed, the tubes are slender ($L_i/D_i \gg 1$), and the angles of confluence are all equal to 90°. The architecture is defined by six dimensions, three lengths (L_1, L_2, L_3) and three diameters (D_1, D_2, D_3). There are only four degrees of freedom, because of the two constraints (territory, tube volume) that replace equations (2) and (6),

$$2L_2(L_1 + L_3) = A = \text{const} \tag{39}$$

$$L_1 D_1^2 + 2L_2 D_2^2 + L_3 D_3^2 = V = \text{const} \tag{40}$$

The resistance of each tube (R_i) is proportional to the geometric group L_i/D_i^4 ($i = 1, 2, 3$). The total resistance encountered by the flow from $P = \Delta P$ to $P = 0$ is proportional to R_t, where

$$R_t = R_3 + \left(R_1^{-1} + 2R_2^{-1}\right)^{-1} \tag{41}$$

where $R_i = L_i/D_i^4$. For the proper nondimensionalization of the problem we note that the tube length scale follows from the A constraint ($L_i \sim A^{1/2}$), and the diameter length scale is governed by the V constraint, $D_i^2 \sim V/L_i \sim V/A^{1/2}$. The problem statement is placed in dimensionless form by using the dimensionless variables

$$\widetilde{L}_i = \frac{L_i}{A^{1/2}}, \qquad \widetilde{D}_i = \frac{D_i}{V^{1/2}A^{-1/4}}, \qquad \widetilde{R}_t = \frac{R_t}{A^{3/2}V^{-2}} \tag{42}$$

We minimized $\widetilde{R}_t$ numerically by varying the six dimensions subject to the two constraints. We did this in two steps. First, we used the constraints and expressed $\widetilde{R}_t$ as a function of only four variables. Second, we constructed four nested optimization loops, in which we optimized, in order, $\widetilde{D}_1$, $\widetilde{D}_2$, $\widetilde{D}_3$ and $\widetilde{L}_2$. We used the two constraints to calculate $\widetilde{L}_1$ and $\widetilde{L}_3$ during each iteration. The minimized value of $\widetilde{R}_t$ was retained only if the calculated $\widetilde{L}_1$ and $\widetilde{L}_3$ were positive. The numerical method guaranteed accuracy of at least 0.8 percent [13].

The optimized geometry is reported graphically in *figure 7*. Its main feature is the complete disappearance of the stem tube L_3. When the lateral tubes of the cross L_2 are free to move, i.e. when the center of the cross is not fixed, then the easiest route for the flow is through two L_2 tubes positioned closest to the exit. The third tube (L_1) is almost absent: ($D_1/D_2 = 0.14$ in *figure 7*). This degeneracy is similar to the disappearance of the stem in the Y-tube optimization of *figure 4*. The rest of the geometry of *figure 7* is characterized by $L_1/(2L_2) = 0.99$, and $D_3/D_2 = 1$.

More meaningful as an engineering construct is the cross where all four tubes are present. This requires an additional (a third) constraint: fixing the position of the center of the cross relative to the frame of A. As an example, we place the center of the cross in the center of A,

$$L_1 = L_3 \tag{43}$$

and repeat the numerical optimization. This time there are three degrees of freedom represented by three nested optimization loops in the sequence $\widetilde{L}_1$, $\widetilde{D}_3$ and $\widetilde{D}_2$. The positive value of $\widetilde{L}_3$ is guaranteed by equation (43). The

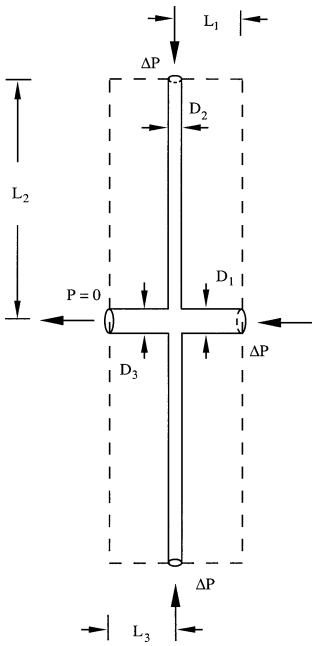

Figure 8. Optimized cross-shaped assembly of tubes when the center of the cross is placed in the center of the A territory.

two constraints allowed us to verify the values of $\widetilde{L}_2$ and $\widetilde{D}_1$ during each iteration. Again, we retained only the minimized values of $\widetilde{R}_t$ for which the calculated $\widetilde{L}_2$ and $\widetilde{D}_1$ values are positive. The numerical method had an accuracy of at least 0.65 percent [13]. The optimized geometric features of the assembly are drawn to scale in *figure 8*.

7. OTHER DUCT MATERIAL CONSTRAINTS

In all the examples treated until now we invoked the total duct volume constraint, equation (6). This constraint is appropriate in flow systems where the volume fraction occupied by ducts is at a premium. This is certainly the case in living systems (e.g., lungs, vascularized tissues), where incentives are great for packing the volume with solid tissue that performs metabolic and motor functions. Not surprisingly, the volume constraint originates from physiology [3, 4, 11, 12], where its invocation is frequent and not questioned.

Similar applications are found in engineering, as in the cooling of electronics packages with single-phase fluid ducted through optimally sized and positioned channels [14]. Here, again, the incentive is to build the most electronics possible into the volume — the most working solid — and this puts pressure on the designer to limit the volume fraction set aside for fluid.

The minimization of construction and operating costs is the ultimate optimization basis in engineering. Approached from this point of view, the constraint that accounts for the ducts in the present problems assumes forms similar to but not exactly the same as equation (6). In the important field of urban hydraulics [15–20], for example, the cost of a network of ducts (lengths L_i, widths D_i) is driven by the amount of duct wall material ($\sim \sum_i L_i D_i$). For this reason, in place of equation (6) we also considered the wall material and/or excavated soil constraint. For the T-shaped assemblies of *figures 1* and *2* the new material constraint is the volume of excavated soil

$$V = (L_1 D_1 + 2L_2 D_2)z \tag{44}$$

where z is the depth of excavation. Repeating the two-step geometric optimization of the T-shaped assembly with round tubes and fully-developed laminar flow (section 2) we obtain the aspect ratios

$$\frac{D_2}{D_1} = 2^{-2/5}, \qquad \frac{L_2}{L_1} = 2^{-3/5} \tag{45}$$

These ratios are comparable with but not the same as those derived earlier, equations (11) and (17). The duct material constraint does matter.

This conclusion finds reinforcement in the results obtained by repeating the three-step optimization of the T-shaped assembly of ducts (not necessarily round) with fully-developed and fully-rough turbulent flow (section 3). When the duct material constraint (44) replaces equation (6), the optimized aspect ratios (24) and (26) are replaced, in order, by

$$\frac{D_2}{D_1} = 2^{-1/2}, \qquad \frac{L_2}{L_1} = 2^{-1/2} \tag{46}$$

These ratios are not the same as in equations (24) and (26). Furthermore, equations (46) show that D_2/D_1 is equal to L_2/L_1. When the duct volume constraint (6) was used, this coincidence occurred in the case of fully-developed laminar flow (section 2), cf. equations (11) and (17).

8. T-SHAPED ASSEMBLY OF TUBES FOR THE DISTRIBUTION OF HOT WATER

An interesting class of problems that may be viewed as being superimposed on the flow problems considered

until now, is the distribution of hot water over a given territory. The importance of this problem has been recognized in studies where the layout of the water flow over the territory is assumed [21]. In the present approach the layout (e.g., aspect ratio of the territory covered by the T-shaped construct) is one of the features to be optimized, and is deduced based on the minimization of the overall resistance to fluid flow. An additional optimization opportunity is offered by the question of how to distribute over the ducts a given amount of thermal insulation so that the temperature of the hot water that is being delivered is maximum.

For illustration, consider again the T-shaped assembly of round tubes with laminar flow (section 2), *figure 1*. Hot water of temperature T_0 enters the L_1 tube from the left, reaches the temperature T_j at the junction with the L_2 tubes, and exits with the temperature T_{out}. The temperature decreases along the flow length because of the loss of heat to the ambient (T_∞). Assume that the dominant thermal resistance between the water stream and the ambient is due to the cylindrical shell of insulation wrapped around each pipe. The rate of heat loss per unit of pipe length is

$$q' = \frac{2\pi k(T - T_\infty)}{\ln(r_o/r_i)} \tag{47}$$

where r_i and r_o are the inner and outer radii of the insulation layer (*figure 9*), $T(x)$ is the temperature distribution along the stream (or along the r_i wall), x is the longitudinal coordinate, and k is the thermal conductivity of the insulating material. To obtain the temperature distribution $T_1(x)$ along the L_1 tube we write the first law for the tube element of length dx,

$$-\dot{m}c_p\, dT_1 = q'\, dx \tag{48}$$

and integrate using equation (47) and $T_1 = T_0$ at $x = 0$,

$$\frac{T_1(x) - T_\infty}{T_0 - T_\infty} = \exp\left(-\frac{c_1 x}{\dot{m}c_p}\right) \tag{49}$$

where c_1 is the conductance factor appearing in equation (47),

$$c_1 = \frac{2\pi k}{\ln(r_o/r_i)_1} \tag{50}$$

In particular, the junction temperature corresponds to setting $x = L_1$ in equation (49),

$$\frac{T_j - T_\infty}{T_0 - T_\infty} = \exp\left(-\frac{c_1 L_1}{\dot{m}c_p}\right) \tag{51}$$

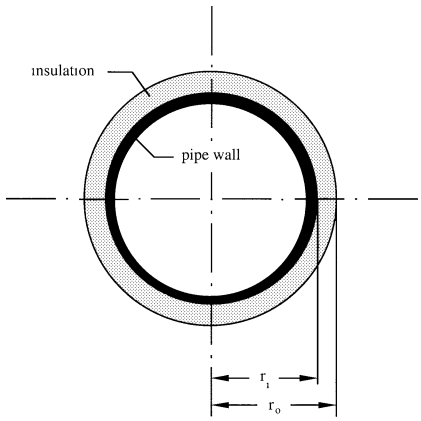

Figure 9. Geometry of insulation shell on a round pipe.

The same analysis delivers the temperature distribution $T_2(y)$ along one of the L_2 tubes, where y is measured away from the junction,

$$\frac{T_2(y) - T_\infty}{T_j - T_\infty} = \exp\left(-\frac{c_2 y}{(\dot{m}/2)c_p}\right) \tag{52}$$

Note the index 2, which accounts for properties of the L_2 stream. Note also the flow rate $\dot{m}/2$ through the L_2 tubes. The water exit temperature is $T_{out} = T_2(L_2)$, cf. equation (52),

$$\frac{T_{out} - T_\infty}{T_j - T_\infty} = \exp\left(-\frac{c_2 L_2}{(\dot{m}/2)c_p}\right) \tag{53}$$

Finally, by eliminating T_j between equations (53) and (51) we obtain the outlet temperature as a function of the distribution of thermal insulation,

$$\frac{T_{out} - T_\infty}{T_0 - T_\infty} = \exp\left[-\frac{1}{\dot{m}c_p}(c_1 L_1 + 2c_2 L_2)\right] \tag{54}$$

To maximize T_{out} is to minimize the group $(c_1 L_1 + 2c_2 L_2)$, or

$$F = \frac{L_1}{\ln(r_o/r_i)_1} + \frac{2L_2}{\ln(r_o/r_i)_2} \tag{55}$$

subject to the fixed amount of insulation,

$$V = \pi\left(r_o^2 - r_i^2\right)_1 L_1 + 2\pi\left(r_o^2 - r_i^2\right)_2 L_2 \tag{56}$$

This constraint can be rearranged to show explicitly the role played by the radii ratios $(r_o/r_i)_{1,2}$,

$$\frac{V}{\pi r_{i1}^2} = \left[\left(\frac{r_o}{r_i}\right)_1^2 - 1\right] L_1 + 2f^2\left[\left(\frac{r_o}{r_i}\right)_2^2 - 1\right] L_2 \tag{57}$$

where f is the step change in pipe radius (or diameter) that takes place at the junction,

$$f = \frac{r_{i2}}{r_{i1}} = \frac{D_2}{D_1} < 1 \tag{58}$$

This ratio is known from the minimization of flow resistance subject to total tube volume (section 2), or total tube wall material (section 7). The minimization of F with respect to $(r_o/r_i)_{1,2}$ and subject to the insulation constraint (57) yields

$$\frac{(r_o/r_i)_1}{(r_o/r_i)_2} = f < 1 \tag{59}$$

In conclusion, the smaller tubes (L_2) must have larger r_o/r_i ratios, i.e. relatively thicker shells of thermal insulation. The analysis that led us to this conclusion can be repeated if a more realistic model of the heat loss process is required. For example, the heat loss model (47) is based on the assumption that the thermal resistance between the hot fluid and the ambient is dominated by the shell of insulating material, $\ln(r_o/r_i)/(2\pi k)$. Now that the ratio r_o/r_i has been determined, equation (59), it is important to check the validity of the dominant resistance assumption,

$$\frac{\ln(r_o/r_i)}{2\pi k} \gg \left(\frac{t_w}{2\pi r_i k_w}, \frac{1}{2\pi r_o h}\right) \tag{60}$$

where t_w and k_w are the specified pipe wall thickness and thermal conductivity, and h is the convective heat transfer coefficient between the outer surface of the insulation and the ambient.

9. CONCLUSIONS

In this paper we applied the method of thermodynamic optimization to several classes of simple flow systems consisting of T- and Y-shaped assemblies of ducts, channels and streams. In each case, the objective was to identify the geometric configuration that maximized performance subject to several global constraints. In pure fluid flow (e.g., *figures 1* and *2*) the maximization of thermodynamic performance reduced to the minimization of resistance to fluid flow, or the minimization of entropy generation when the flow rate is prescribed. In systems with multiple functions such as the distribution of hot water over a territory (section 8), the maximization of global performance is a combination of minimizing fluid-flow resistance and the total loss of heat from the pipe assembly.

The relatively simple constructs, and the various formulations of the global performance maximization problem were chosen intentionally in order to stress the most important features of the method. First is the emergence of geometric structure as a result of the consistent maximization of performance subject to constraints. From the T-shaped construct with laminar flow (*figure 1*) to the distribution scheme for hot water (section 8), every detail of the optimal flow geometry was a result of the pursuit of better global performance subject to global constraints. Geometry matters, and its optimal selection (design, architecture) is the key to achieving superior performance.

Another important feature illustrated by these examples is the robustness of the optimized designs. For example, in sections 2 and 3 we saw that the optimal ratio of channel thicknesses (D_2/D_1) is completely independent of the rest of the geometric parameters and global constraints. Robustness, and the physical parameters with respect to which the optimized structure is relatively insensitive are very important in practice. They simplify the design of future and more complex systems, and, at the same time, they insure a near-optimal performance of existing systems the structures of which may deviate from the originally intended design.

Another example of robustness is the flow resistance minimized in sections 2 and 3. In laminar flow, following the two-way optimization presented in equations (5)–(17), we find that the twice-minimized resistance R_{mm} can be expressed in terms of the tube volume V and plane territory A,

$$R_{mm} = 4\frac{A^{3/2}}{V^2} \tag{61}$$

The corresponding conclusion for the optimization of the T-shaped construct with turbulent flow (section 3) is

$$R_{mm} = 4\frac{A^{7/4}}{V^{5/2}} \tag{62}$$

These two R_{mm} functions, equations (61) and (62), are surprisingly close even though their respective flow regimes are drastically different.

The constraints are also essential in the pursuit of the unknown, which is the optimal flow geometry. Constraints are not boundary conditions. The boundaries are the unknowns, the architecture to be optimized. Constraints are global concepts that must be recognized from the beginning, in the same step as the global objective. The constraint type affects the resulting geometry, as shown by the duct wall material constraints (section 7) in comparison with the duct volume constraint (section 2).

Constraints also affect the meaningfulness of the results, as shown in the degenerate examples of sections 5 and 6.

Throughout this series of examples we saw that the optimized geometry has the effect of "partitioning" optimally certain features of the system, e.g., pressure drop, flow resistance, amount of thermal insulation, etc. Optimal partitioning, or optimal allocation of constrained quantities is a by-product of the optimization of flow geometry. It is encountered every time global performance is maximized: optimal allocation is another way of interpreting the spatial optimization of the flow arrangement, i.e. *the optimal spreading of imperfection* (flow resistances, irreversibilities) such that the entire system performs as well as the constraints might allow it to perform.

More fundamentally, the sequence in which the examples were presented in this paper holds an important message for future applications of the method. We started with examples of pure fluid flow, because they are the simplest: they suffer from only one irreversibility mechanism, fluid friction. Examples of pure heat flow are already documented in the literature. The paper ended with an example of combined heat and fluid flow (section 8), where the objective was to distribute hot water over a territory. This problem can be reformulated in terms of distributing a flow other than hot water, for example, exergy or a stream of goods. The message is that the method of optimal allocation of streams over an area can and should be introduced in other fields (exergy analysis, thermoeconomics) in the way in which it was introduced in urban hydraulics in section 8.

REFERENCES

[1] Bejan A., Tsatsaronis G., Moran M., Thermal Design and Optimization, Wiley, New York, 1996.

[2] Feidt M., Thermodynamique et optimisation énergetique des systèmes et procedés, Technique et documentation, Lavoisier, Paris, 1987.

[3] Weibel E.R., Morphometry of the Human Lung, Academic Press, New York, 1963.

[4] MacDonald N., Trees and Networks in Biological Models, Wiley, Chichester, UK, 1983.

[5] Scheidegger A.E., Theoretical Geomorphology, 2nd edition, Springer-Verlag, Berlin, 1970.

[6] Schumm S.A., Mosley M.P., Weaver W.E., Experimental Fluvial Geomorphology, Wiley, New York, 1987.

[7] Bejan A., Int. J. Heat Mass Tran. 40 (1997) 799–816.

[8] Bejan A., Rev. Gén. Therm. 36 (1997) 592–604.

[9] Bejan A., Dan N., J. Heat Tran. 121 (1999) 675–682.

[10] Bejan A., Ledezma G. A., Physica A 255 (1998) 211–217.

[11] Murray C.D., Proc. Acad. Nat. Sci. 12 (1926) 207–214.

[12] Thompson D'A.W., On Growth and Form, Cambridge University Press, Cambridge, UK, 1942.

[13] Taylor J.R., Introduction to error analysis, 2nd edition, University Science Books, Sausalito, CA, 1997.

[14] Bejan A., Sciubba E., Int. J. Heat Mass Tran. 35 (1992) 3259–3264.

[15] Padet J., Fluides en écoulement, méthodes et modèles, Enseignement de la Physique, Editions Masson, 1991.

[16] Deb A.K., J. Env. Engrg. Div., Proc. ASCE 99 (1973) 405–409.

[17] Alperovits E., Shamir U., Water Resources Res. 13 (1977) 885–900.

[18] Deb A.K., J. Env. Engrg. Div., Proc. ASCE 100 (1974) 821–835.

[19] Wilson A.J., Britch A.L., Templeman A.B., Engrg. Optimization 1 (1974) 111–123.

[20] Mays L.W., Yen B.C., Water Resources Res. 11 (1975) 37–47.

[21] Barreau A., Moret-Bailly J., Entropie 75 (1977) 21–28.